Rossby Wave Radiation in the Cape Verde Frontal Zone*

MICHAEL A. SPALL

Woods Hole Oceanographic Institution, Woods Hole, Massachusetts

(Manuscript received 21 May 1991, in final form 4 November 1991)

ABSTRACT

Radiating baroclinic Rossby waves excited through instability of the Cape Verde frontal zone are proposed as a mechanism for the generation of mesoscale variability at middepth (1000 m) in the southeastern North Atlantic basin. Linear quasigeostrophic theory is applied to an idealized front representative of the Cape Verde frontal zone to demonstrate that the front is unstable to modes that may radiate away from the frontal region as baroclinic Rossby waves. Evidence for the existence of these waves is obtained from an eddy-resolving, basin-scale general circulation primitive equation model. In addition, the model fields are used to identify characteristic signatures of the waves in terms of quantities that may be directly observed in the ocean. Lagrangian trajectories, Reynolds stress, eddy kinetic energy, and frequency spectra taken from SOFAR float and current-meter records are all in good agreement with the amplitude and distribution implied by the wave radiation in both the linear theory and the full primitive equation model. It is concluded that the Cape Verde frontal zone is a source of radiating baroclinic Rossby waves and that these waves are an important component of the low-frequency eddy energy at the middepth ocean in the southeastern basin.

1. Introduction

Mesoscale variability may be introduced to the mid-ocean through the radiation of Rossby waves generated at distant meandering frontal regions (Pedlosky 1977). Increased mesoscale activity in the vicinity of strong currents has often been related to baroclinic and/or barotropic instabilities of these fronts. Talley (1983) notes that the most unstable modes of a zonal current are often trapped within a deformation radius of the source region, but that modes with lower growth rates are sometimes able to radiate away from the jet. The process has been most often investigated in the context of western boundary currents such as the Gulf Stream and Kuroshio. Early theories for steady meander amplitude or exponential growth indicated that the phase speed of the meanders had to be westward in order to radiate Rossby waves into motionless interiors (i.e., Pedlosky 1977; Talley 1983). More recently, Malanotte-Rizzoli et al. (1987) and Hogg (1988) have shown that westward-propagating Rossby waves may be generated by eastward-propagating meanders if the meanders have periods of growth and decay.

Observational evidence for Rossby wave radiation is growing. Several isolated observations of Rossby waves have been related to Gulf Stream meandering or ring formation events (Louis et al. 1982; Johns and Watts 1986; Schultz 1987). Bower and Hogg (1991) find some evidence of wave radiation to the north of the Gulf Stream in historical current-meter data. Satellite altimeter observations in the Kuroshio region have also shown evidence of wave radiation (Tai and White 1990).

Although these previous results have been sometimes supportive of radiation as a mechanism of generating variability away from frontal regions, they are far from conclusive and, to date, have been limited to strong western boundary current regions. This bias results from having considerably more data available in these regions and the fact that strong fronts might be expected to radiate waves more strongly than weak fronts, making these regions likely places to observe radiating waves. There are several factors that work against observing wave radiation near western boundary currents, including complex topography (which may change the propagation characteristics of the waves), energetic variability due to other processes (i.e., local instabilities, surface forcing, and mesoscale eddies and rings), and a complex wave radiation mechanism that may depend on the transient nature of the meander amplitudes. These factors do not compete with wave radiation as strongly in the Cape Verde frontal zone because the topography is relatively smooth, the eddy kinetic energy is low, and the frontal flow is to the west (conducive to westward meander phase speeds).

A schematic of the upper ocean currents in the eastern basin of the North Atlantic is shown in Fig. 1. The region of interest for the present study is indicated by

* Woods Hole Oceanographic Contribution Number 7709.

Corresponding author address: Dr. Michael A. Spall, Woods Hole Oceanographic Institution, Clark 311 A, Woods Hole, MA 02543.

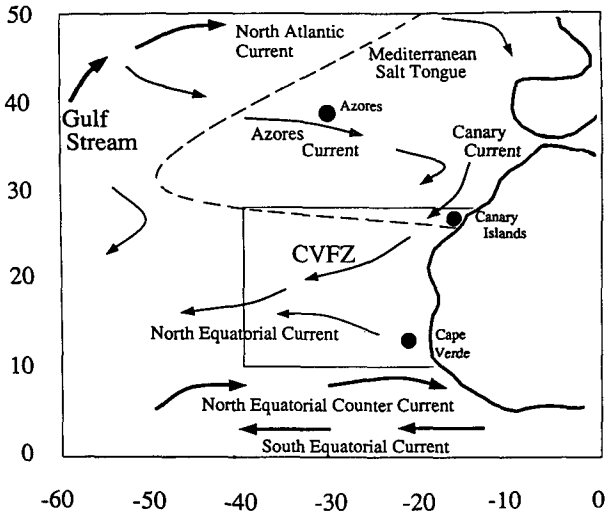

FIG. 1. Schematic of upper ocean currents in the eastern basin.

the boxed area extending from 40°W to the coast and from 10°N to 28°N. In addition to the general Sverdrup circulation, there are two major fronts located in this area, the Azores Current and the Cape Verde frontal zone. The Azores Current originates near the Grand Banks where the Gulf Stream bifurcates into the northeastward-flowing North Atlantic Current and the southeastward Azores Current. Once in the Canary Basin the current filaments, turns to the south, and recirculates toward the west. The term Cape Verde frontal zone (CVFZ) was introduced by Zenk et al. (1991) to characterize the eastern portion of the water mass boundary between the North Atlantic central water and the South Atlantic central water. It is located between 15°N and 25°N in this area. There are two upper ocean currents located in the CVFZ. The Canary Current flows to the south along the coast of Africa, separates from the coast at about 23°N, and flows to the west. This westward flow merges with the upper ocean wind-driven transport from the south to form the westward-flowing North Equatorial Current. For reference, the Mediterranean salt tongue is also indicated on the figure by the dashed line; it is located primarily to the north of the region of interest. Just to the south of the boxed area are the eastward-flowing North Equatorial Counter Current and the westward-flowing South Equatorial Current. The Azores, Cape Verde, and Canary Islands are also indicated.

The mesoscale variability of the eastern North Atlantic has been the subject of much research in recent years. Although the eastern basin was traditionally thought to be governed primarily by Sverdrup dynamics, recent observational programs have revealed the existence of relatively strong upper ocean fronts, mesoscale eddies, and submesoscale lenses of Mediterranean water. Much of the modeling and theoretical work has been concentrated on the dynamics of the two strongest fronts in the region, the Azores Current and the CVFZ. This interest results from both the predominance of instability theory as an eddy generation mechanism and the availability of data in the upper ocean near these fronts. Linear theory and numerical models have demonstrated that these frontal regions are subject to baroclinic instability. The observed space and time scales of variability are consistent with those predicted by the stability models. Only recently has enough data been collected to characterize the mesoscale variability in the deep ocean and away from these frontal regions.

The present analysis proposes radiating baroclinic Rossby waves excited through instability of the CVFZ as a mechanism to generate mesoscale variability in the midocean (1000 m) southeastern basin. We initially make use of linear quasigeostrophic theory to characterize the space and time scales of the waves that may be forced by the frontal instability. An eddy-resolving, general circulation primitive equation model is then used to demonstrate that the frontal instability does generate waves consistent with the linear theory and that these waves radiate into the relatively quiescent regions adjacent to the front. In addition, the model fields are used to identify characteristic signatures of the waves in terms of quantities that may be directly observed in the ocean. Lagrangian trajectories, Reynolds stress, eddy kinetic energy, and frequency spectra taken from observations are all in good agreement with the amplitude and distribution generated by the wave radiation in both the linear theory and the full primitive equation model.

A linear quasigeostrophic stability analysis is carried out in section 2 to demonstrate that the CVFZ is capable of generating baroclinic Rossby waves. The existence of radiating waves and their characteristic signature in a general circulation primitive equation model are presented in section 3. Observational evidence of radiating Rossby waves is given in section 4 and final conclusions are presented in section 5.

2. Rossby wave radiation

A frontal jet may be the source of radiating waves if a wavelength and phase speed of the frontal instability coincide with a point on the dispersion curve for a wave in the surrounding medium (Talley 1983). Waves characterized by such a point might then be expected to be found radiating away from the region of frontal instability. The unstable wavelength does not need to be the fastest-growing instability of the jet; it only has to have a growth rate large enough to generate a detectable perturbation. Westward jets, such as the CVFZ, are generally more likely to have unstable waves with westward phase speeds than are eastward jets. For this reason, it is also more likely that a westward jet may match the Rossby wave dispersion relation and generate disturbances that are able to radiate away from

the frontal region. We demonstrate here that an idealized model of the CVFZ satisfies this requirement.

A linear quasigeostrophic stability analysis is applied to a baroclinic jet in a zonal channel on the beta plane with periodic boundary conditions in the downstream direction. The linear form of quasigeostrophic equations is written in terms of the streamfunction ψ as

$$\nabla^2\psi_t + \beta\psi_x - f_0 w_z = 0 \quad (1)$$

$$\psi_{zt} = (N^2/f_0)w. \quad (2)$$

The mean density profile and velocity structure of the jet are intended to represent the unperturbed state of the CVFZ. The background stratification is taken to be the same as that used in the numerical study of Onken and Klein (1991, hereafter OK91) and is shown in Fig. 2a. The velocity structure of the unperturbed jet is shown in Fig. 2b. The vertical shear at the center of the jet is based on the analysis of OK91, numerical model calculations (see next section), and the hydrographic data of Zenk et al. (1991). The jet is strongly surface intensified, with a maximum westward velocity of 8.6 cm s^{-1} at the surface and 2 cm s^{-1} at 400 m. The horizontal profile is taken to be Gaussian with an e-folding scale of 100 km. The results of the following stability analysis are not overly sensitive to reasonable choices of these jet parameters.

These reference density and velocity profiles define a mean state streamfunction $\Psi(y, z)$ that together with a perturbation streamfunction $\phi(x, y, z, t)$, defines the total streamfunction. Following the analysis of Beckmann (1988), the perturbations are assumed to have a zonal wave form of

$$\phi = M(y)F(z)\exp[i(kx - \omega t)]. \quad (3)$$

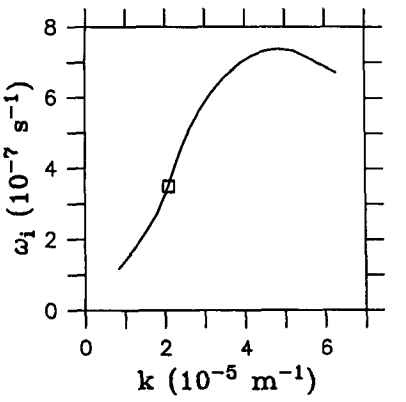

FIG. 3. Growth rate for most unstable mode with westward phase speed; CME Rossby wave packet wavelength is indicated by the square.

Substitution of this form into Eqs. (1) and (2) results in an eigenvalue problem for the complex frequency $\omega = \omega_r + i\omega_i$. The system of equations is solved using second-order finite differences in the horizontal and Chebyshev polynomials in the vertical. The perturbation is also assumed to be periodic in the meridional direction. Details of the solution procedure can be found in Beckmann (1988). The horizontal grid spacing is 7.8 km and nine polynomials are used in the vertical. The bottom depth is constant at 4500 m, and the environmental rotation parameters are representative of conditions at 20°N, $f_0 = 0.5 \times 10^{-4}$ s^{-1}, and $\beta = 2.0 \times 10^{-11}$ m^{-1} s^{-1}.

For each wavenumber k, unstable modes may exist with growth rate ω_i and phase speed $c = \omega_r/k$. We are interested only in those modes that have a westward

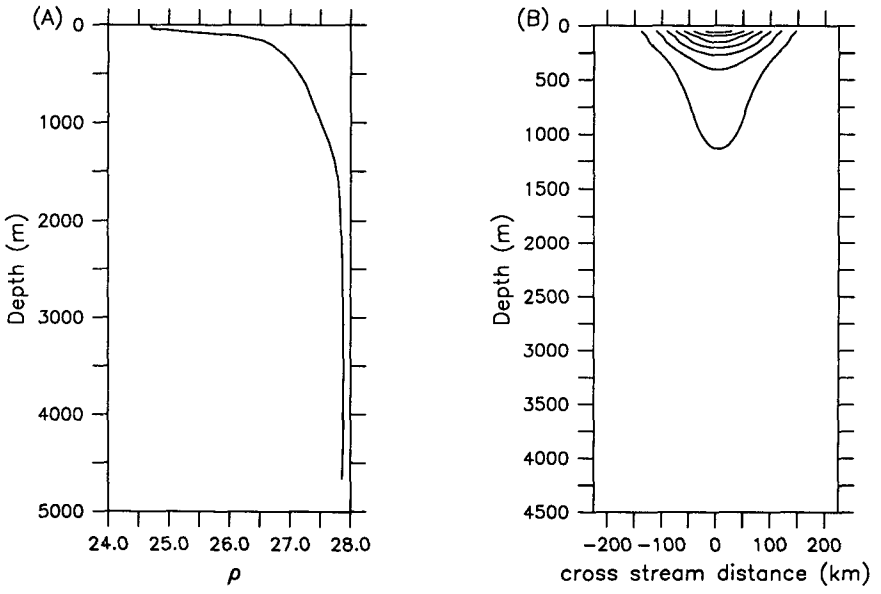

FIG. 2. (a) Background density profile and (b) unperturbed velocity profile for stability analysis (contour interval: 1 cm s^{-1}).

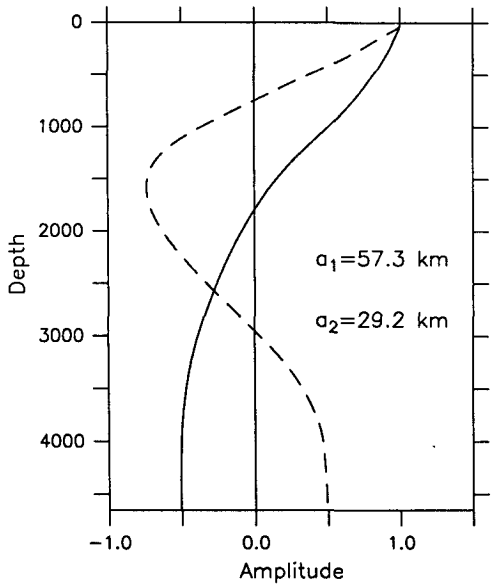

FIG. 4. First two baroclinic modes. Deformation radii are 57.3 km and 29.2 km.

phase speed in order to determine if they force Rossby waves in the surrounding water. Figure 3 shows the growth rate for the fastest-growing mode with westward phase speed at each wavenumber. The jet profile is unstable to westward-propagating disturbances between wavenumbers 8.4×10^{-6} m^{-1} and 6.3×10^{-5} m^{-1}, or wavelengths between 100 km and 750 km. The fastest-growing perturbation with westward phase speed is found at 140-km wavelength, slightly less than the 200-km wavelength reported by OK91 for a uniform vertical shear. The growth rate decreases for wavelengths longer than 140 km; however, wavelengths up to 400 km have substantial growth rates that remain within a factor of 3 of the fastest-growing waves.

To determine if Rossby wave radiation from the front is likely, the dispersion relation for freely propagating waves in the surrounding water must be calculated. The dispersion relation for a baroclinic Rossby wave is written as

$$\omega_r = -\frac{\beta k}{k^2 + l^2 + \lambda_n} \tag{4}$$

where $\lambda_n = 1/a_n^2$ and a_n is the radius of deformation for the nth baroclinic mode. The first two baroclinic modes are shown in Fig. 4. The first mode has a zero crossing at 1800 m and the second has zero crossings at 750 m and 2950 m. The associated radii of deformation are 57.3 km and 29.2 km. It is assumed that the meridional wavenumber is one half of the zonal wavenumber ($l = 0.5k$; this choice is motivated by observations that are discussed in a later section). The dispersion relations for the first two baroclinic modes of the linear Rossby wave are shown in Fig. 5a. The highest frequency is reached for the first baroclinic mode at wavenumber 1.25×10^{-5} m^{-1}, or a wavelength of 500 km. All waves with wavelengths shorter than 500 km will have an eastward group velocity ($c_{gx} = \partial\omega/\partial k$), and all longer waves will have a westward group velocity. The second baroclinic mode has lower frequency at all wavenumbers.

The phase speeds of the Rossby waves are shown in Fig. 5b. The phase speed for the first baroclinic mode varies from near zero for very short waves to −7 cm s^{-1} (negative phase speeds are to the west) for the longest waves. Also plotted on the figure are the phase speeds of the fastest growing westward-propagating modes obtained from the linear stability analysis (bold line). We find that the perturbation at wavenumber 2×10^{-5} m^{-1} (315 km) has a phase speed that just matches that of a first-mode baroclinic Rossby wave in the surrounding water. Modes of the jet that are unstable to wavenumbers larger than this have westward phase speeds that are faster than can be supported by the baroclinic waves. Jet instabilities that exist at very low wavenumbers have a phase speed much slower than that for the mode 1 waves. The growth rate for

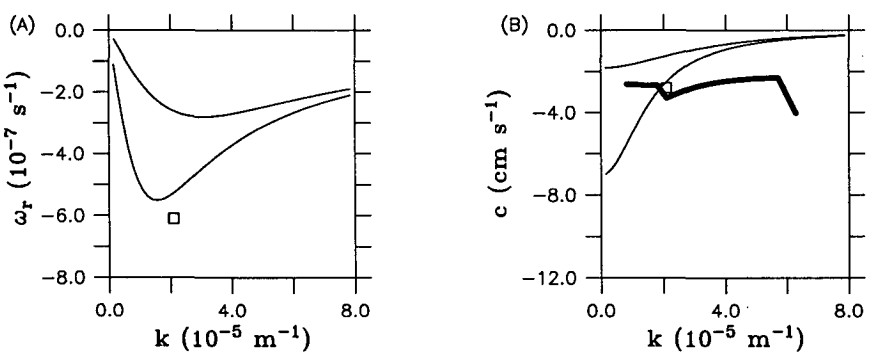

FIG. 5. (a) Dispersion relation for first two baroclinic modes of a Rossby wave and frequency and wavenumber of CME Rossby wave packet (square), (b) phase speed versus wavenumber for first two baroclinic modes; linear stability analysis (bold line) and CME Rossby wave packet (square).

the 315-km wave is found from Fig. 3 to be 3.5×10^{-7} s^{-1}, equivalent to an *e*-folding time of 33 days. For comparison, the *e*-folding time of the fastest-growing wave is approximately half of this, 16 days. Based on this analysis, we expect that the baroclinically unstable CVFZ could generate first-mode baroclinic Rossby waves with wavelengths near 315 km and westward phase speeds of approximately -3 cm s^{-1}. The group velocity is to the east at approximately 1 cm s^{-1}.

Waves generated at the real CVFZ front are not expected to assume the mode 1 profile in the vertical immediately. This is because the CVFZ is more surface intensified than the first baroclinic mode and does not exhibit a strong reversal of flow in the deep. We anticipate that the waves would adjust to this profile through the vertical propagation of energy at the vertical group velocity, approximately 1 km yr^{-1}.

A similar range of baroclinic instability is also found in the numerical study of OK91. Their analysis indicates that the middepth of a periodic zonal jet modeled after the CVFZ is dominated by variability with spatial scales of 125 km to 350 km. The phase speeds of these modes vary from nearly zero for the shortest waves to -3.5 cm s^{-1} for the longest waves. They attribute this variability to baroclinically unstable modes of the system. The phase speed of the 300-km waves in their model is close to that predicted by the linear stability analysis here. This implies that nonlinear effects do not significantly alter the relationship between the phase speed and wavelength of the perturbation at this wavelength. This is important because, for perturbations that have a growth rate shorter than the period of the wave (as in the present analysis), we expect radiation of energy in the form of Rossby waves to take place in the nonlinear regime. Thus, in the following analysis, it is assumed that the frequency of the frontal perturbations that radiate waves is real, not imaginary as it is in the linear stability analysis.

It is noted here that OK91 do not discuss the possibility of radiating waves, but do demonstrate the presence of long barotropic Rossby waves (very rapid westward phase speeds) and topographic Rossby waves (bottom trapped with eastward phase speeds). It is possible that radiating waves were not detected in their simulation because the time scales needed for the waves to propagate away from the source region are longer than the time scales for which their periodic model was run.

3. Numerical simulations

The previous analysis indicates that the CVFZ may be a source region for baroclinic Rossby waves. We will now seek evidence of such wave generation and propagation in an eddy-resolving, primitive equation general circulation model. The calculation is an extension of the original Community Modelling Effort (CME) calculation (Bryan and Holland 1989), carried out at the National Center for Atmospheric Research, in which the horizontal and vertical diffusion parameterizations have been reduced. All other aspects of the extended simulation are the same as in the original CME calculation. The model domain extends from 15°S to 65°N and has eddy-resolving horizontal resolution (1/3° latitude, 2/5° longitude) and 30 levels in the vertical. The model was initialized with climatological hydrography and integrated for 25 years. Details of the numerical simulation can be found in the preceding reference and are not reproduced here. Such a basin-scale general circulation model is desirable to study the generation and propagation of these waves because the time scales required for the waves to extend away from the frontal zone into the interior is on the order of years. Idealized periodic models, such as that used by OK91, are valid only for relatively short time scales, on the order of months, so they are not as appropriate for the present analysis.

The mean hydrography of the numerical simulation in this region compares well with climatology (Spall 1990, hereafter S90). The CVFZ separates the saline, warm North Atlantic central water to the north from the fresher, colder South Atlantic central water to the south (see Fig. 1). It has been shown that this front is baroclinically unstable (S90; OK91). This front also marks the boundary between the ventilated thermocline circulation of the North Atlantic and the unventilated shadow zone of Luyten et al. (1983).

Although baroclinic waves would be expected to have a signal throughout the water column, we will concentrate on the middepths (1000 m) for two reasons. First, the amplitude of the waves is expected to be small, so that their signal in the upper ocean may be obscured by other mesoscale phenomena that are surface intensified. Second, this depth is relevant to the Mediterranean outflow and both Lagrangian float and moored instrument data are available here. The zero crossing of the first baroclinic mode is at 1800 m. The amplitude at 1000 m is approximately half its maximum at the surface (Fig. 4) so we expect to have a strong signal at this depth.

Fig. 6 shows the velocity field at 1125 m over an 8° square centered at 20°N, 27°W on day 3 of year 22 in the model. This pattern of mesoscale variability is typical of that found to the north of the CVFZ at this depth. The eddies have velocities up to 5 cm s^{-1} and spatial scales on the order of 150 km. A time series of such plots indicates that cyclonic and anticyclonic eddies near 19.5°N, 26°W move to the southwest. It is not obvious from the velocity field alone what the nature and source of this variability is.

Analysis of the vorticity equation terms consistent with the model numerics (Spall 1989) in this region demonstrates that these eddies constitute a baroclinic Rossby wave packet. The dominant balance in the vorticity equation for a linear, baroclinic Rossby wave is

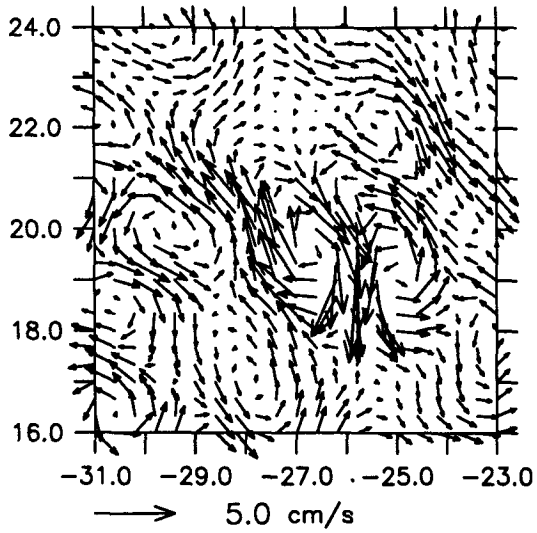

FIG. 6. Instantaneous velocity field at 1125 m from CME calculation.

$$\nabla^2\psi_t = -\beta\psi_x + w_z f. \tag{5}$$

Figures 7a–d show the relative vorticity ($\nabla^2\psi$), the time change of relative vorticity ($\nabla^2\psi_t$), horizontal advection of planetary vorticity ($-\beta\psi_x$), and stretching of planetary vorticity ($w_z f$). All other terms in the full primitive equation vorticity balance are found to be negligible. A wave packet can be clearly seen extending from 18°N, 28°W to the northeast near 23°N, 24°W. The Rossby number of the variability is small, O(0.01). The time change of relative vorticity is out of phase with the relative vorticity and indicates southwestward propagation of the wave crests. The wave propagates primarily by advection of planetary vorticity, with a smaller contribution from the vertical stretching term. The stretching is in phase with, but of opposite sign to, the advection term. The vertical velocity in this component of the wave is on the order of 3×10^{-3} cm s^{-1}, much larger than that found at this depth away from the wave.

The wave is characterized by a wavelength of approximately 300 km and a phase speed of -2.8 cm s^{-1}. This gives a frequency of 6×10^{-7} s^{-1}, or a period of approximately 120 days. The location of this wave on the linear Rossby wave dispersion diagram is indicated by the square in Figs. 5a and 5b. It is in reasonable agreement with the linear Rossby wave theory and falls remarkably close to the radiating waves predicted by the stability analysis. Based on this analysis we conclude that this westward-propagating disturbance is a baroclinic Rossby wave.

For a wave packet of the orientation shown in Fig. 7, the meridional wavenumber is of the same sign as the zonal wavenumber and the meridional phase speed is to the south. The meridional group velocity of a linear Rossby wave is always of sign opposite to the meridional phase speed so it is to the north. It was shown from the dispersion curve (Fig. 5a) that the zonal group velocity is to the east, so that energy propagates from the southwest to the northeast in this wave. This is consistent with the CVFZ, which is to the south, being the source of energy for this disturbance. Because the particle trajectories are oriented perpendicular to the direction of phase propagation, the Reynolds stress term ($u'v'$) will be negative for this northeastward group velocity. Southeastward group velocities (where the meridional wavenumber is of opposite sign to the zonal wavenumber) will give a positive Reynolds stress at this wavelength.

The mean Reynolds stress $\overline{u'v'}$ is shown in Fig. 8 at a depth of 1125 m, calculated over the last three years of model integration (the overbar indicates a time average). Also indicated on the figure is the mean position of the CVFZ in the model calculation (long dashed line) and an average of several frontal positions estimated from hydrographic data (Zenk et al. 1991) (short dashed line). To the north of the CVFZ the Reynolds stress is almost everywhere negative while to the south it is almost everywhere positive. The amplitudes are largest approximately 200 km away from the mean position of the CVFZ and indicate energy propagation as far as 600 km to the north and south of the front. As indicated in Fig. 2b, the CVFZ is approximately 300 km wide. This length scale is also in general agreement with the distance at which frontal meanders were found to penetrate into the adjacent motionless regions in the periodic model of OK91. The maximum in Reynolds stress is offset from the mean frontal location because the wave signature dominates the frontal variability only away from the meandering front. The Reynolds stress is found to be very small to the south of the front, east of 26°N. This may be due to the presence of the shallow Cape Verde Plateau and Cape Verde Islands, which would interfere with the wave propagation in this area. The Reynolds stress distribution found here presents strong evidence that these waves exist throughout the region, that the source for these waves is the CVFZ, and that they are indeed radiating waves, propagating energy well away from the front. The symbols indicated on the figure mark the location of observations, which will be discussed in the next section.

To compare these model results with SOFAR float observations, we would like to know what the Lagrangian signature of a float placed in one of these wave packets would look like. The Lagrangian trajectory is recovered from the Eulerian model data (available at 3-day intervals) by inverting the equation.

$$d\mathbf{x}(t; \mathbf{x}_0)/dt = \mathbf{u}(\mathbf{x}(t; \mathbf{x}_0), t) \tag{6}$$

where the vector $\mathbf{x}$ is the three-dimensional particle position, $\mathbf{x}_0$ is the position of the particle at time zero, and $\mathbf{u}$ is the local three-dimensional velocity. This equation is integrated using a fourth-order Runge–

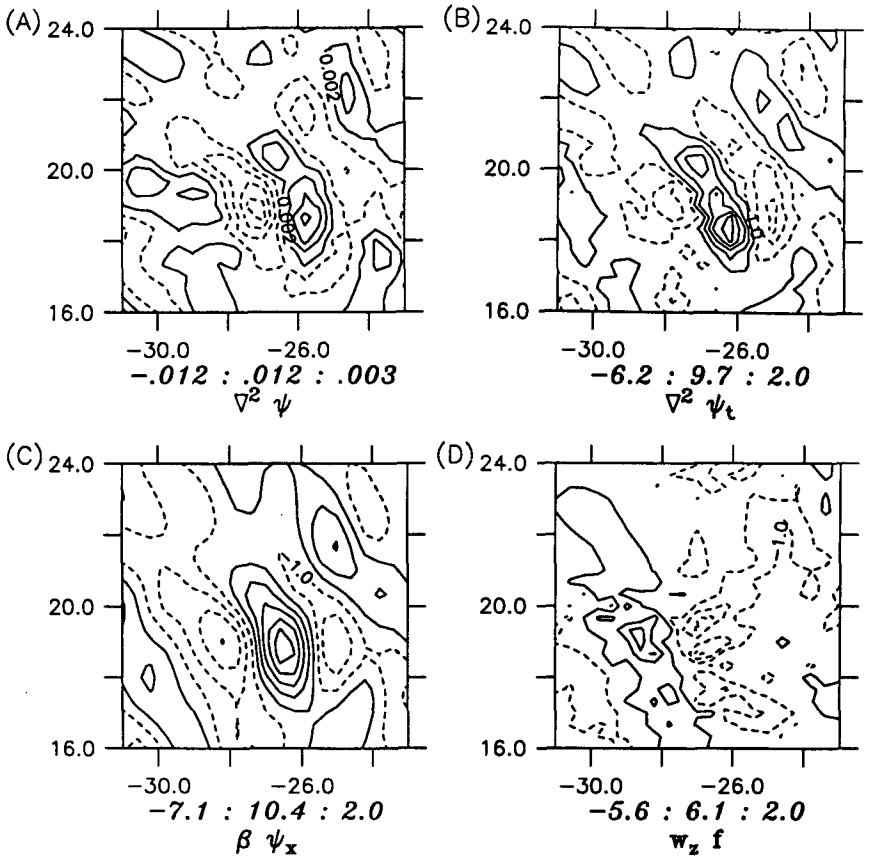

FIG. 7. Vorticity equation terms from CME model calculation, (a) relative vorticity, $\nabla^2\psi$ ($\times 10^{-4}$ s^{-1}), (b) time change of relative vorticity, $\nabla^2\psi_t$ ($\times 10^{-13}$ s^{-2}), (c) advection of planetary vorticity, $-\beta\psi_x$, ($\times 10^{-13}$ s^{-2}), and (d) stretching term, $w_z f$) ($\times 10^{-13}$ s^{-2}).

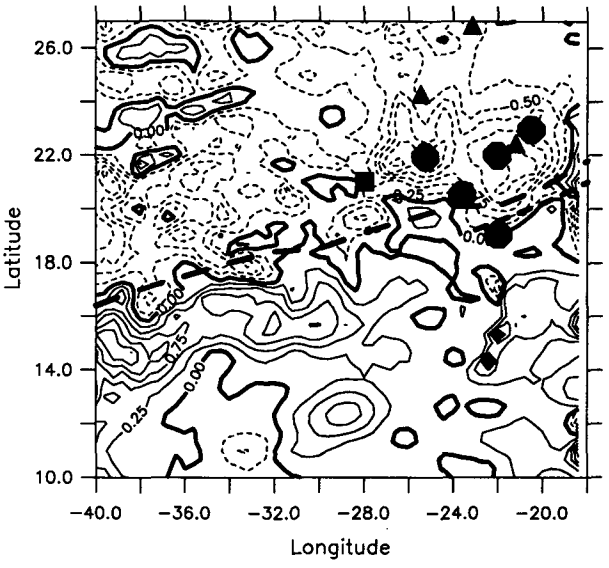

FIG. 8. Reynolds stress ($\overline{u'v'}$) from last three years of CME simulation. Long dashed line indicates mean CVFZ position in CME model; short dashed line indicates mean position from several hydrographic surveys. Square marks mean position for CME float F1; triangles mark mean positions for SOFAR floats FA, FB, and FC; circles mark locations of current meters M1, M2, M3, M4, and M5.

Kütta scheme. The velocity at the location of the Lagrangian water parcel is linearly interpolated from the surrounding (in space and time) model grid points. Model data are provided every 3 days. Böning and Cox (1988) found that Eulerian sampling at 3-day intervals resolved the temporal variability quite well for a Lagrangian analysis in the eastern basin of a primitive equation model with similar resolution. In addition, they found the results to be relatively insensitive to the choice of horizontal interpolation and they also used a linear interpolation in their final analysis.

A simulated float was placed at 21°N, 28°W, at a depth of 1000 m on day 3 of model year 22, near a crest in the wave analyzed previously. The Lagrangian trajectory of this float for the next two years is shown in Fig. 9. A small circle marks the initial position of the float and + marks are placed every 60 days along the float track. Statistics of the float trajectory are summarized in Table 1 for float F1. The mean float position is indicated on the map of Reynolds stress (Fig. 8) by a square. The float demonstrates an oscillating pattern with an amplitude of approximately 150–200 km and an orientation tilted approximately 30° relative to north. Although the float has relatively large advection speeds, up to 5 cm s^{-1}, the net translation over the

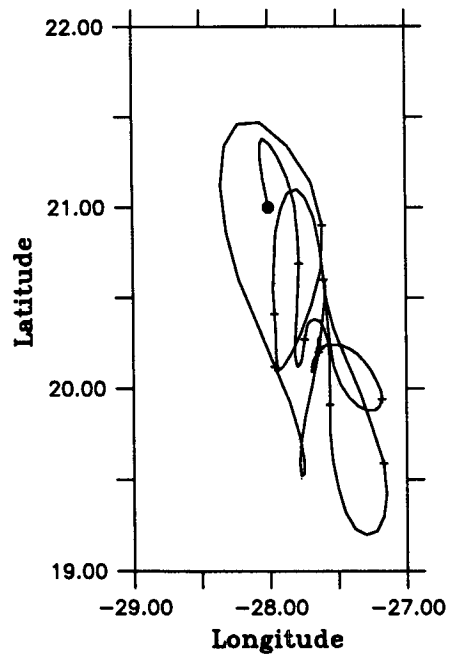

FIG. 9. Two-year Lagrangian trajectory of CME model float F1, circle marks starting point, "+" spaced at 60-day intervals along the trajectory.

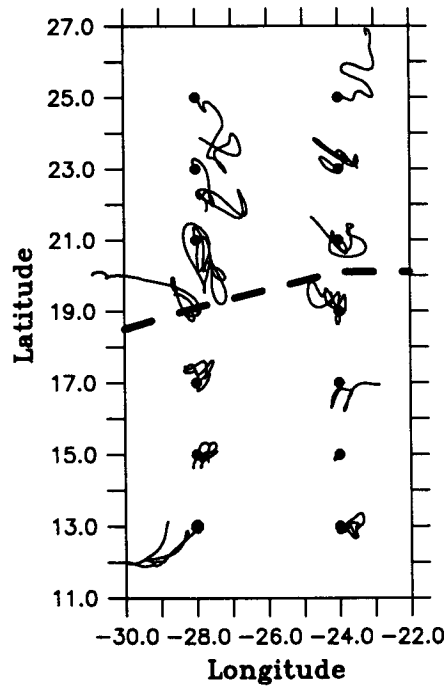

FIG. 10. Two-year Lagrangian trajectories of 14 simulated floats in the CME model.

two years is very small. For a perfect Rossby wave with no mean background flow, we would expect the float to oscillate back and forth parallel to the wave crests, resulting in no net translation over a wave period. The result found here is consistent with such a Lagrangian path. The $\overline{u'v'}$ for this float is -1.1 cm^2 s^{-2}, indicating energy propagation to the north. The model float also upwells (downwells) approximately 100 m as it is advected to the north (south).

If the CVFZ is indeed a source for radiating Rossby waves, we would expect to find them throughout the region both to the north and south of the front, as implied by the map of Reynolds stress shown in Fig. 8. Fourteen floats have been placed in the model fields at two degree spacings along two lines, one line at 28°W and one line at 24°W. The resulting 2-year Lagrangian trajectories are shown in Fig. 10. The mean frontal position in the model is indicated by the dashed line near 18°N. To the north of the front, all floats exhibit some degree of an oscillating pattern with northwest-to-southeast orientation. The floats demonstrate a variety of behavior, including both oscillation and translation (25°N, 24°W), oscillation and ejection from a wave (19°N, 28°W), or advection and entrainment by a passing wave (25°N, 28°W). South of the front, the orientation of the oscillations changes to southwest to northeast, consistent with Fig. 8 and southward energy propagation. This general picture is in agreement with our hypothesis that Rossby waves are present at middepths in this region and that they are generated at the CVFZ. Because almost all floats in this region show some tendency for wavelike behavior, it is also believed that these waves represent the dominant form of eddy kinetic energy at this depth in the model.

Floats placed farther to the north in the model (near 35°N, not shown here) exhibit a very low-frequency (several years), primarily zonal advective path, which is much different from the oscillating patterns seen in

TABLE 1. Summary of statistics for the CME float F1, SOFAR floats FA, FB, FC, and current meters M1, M2, M3, M4, and M5.

Source	Lat (°N)	Long (°W)	Depth (m)	$u'v'$ (cm^2 s^{-2})	EKE (cm^2 s^{-2})
F1	20.1	−27.5	1000	−1.1	4.0
FA	24.5	−25.5	1115	−4.1	6.5
FB	22.4	−21.2	1098	−.33	11.2
FC	26.8	−23.1	1113	−1.6	3.9
M1	19.0	−21.9	1280	1.7	7.4
M2	20.5	−23.6	1255	−1.6	6.7
M3	21.9	−25.3	1200	−4.1	10.9
M4	21.9	−22.0	1307	−5.6	8.3
M5	22.9	−20.5	1292	−1.4	6.1

Fig. 10. Similar zonal advective patterns are also found to the north in the SOFAR float experiment (Zemanovic et al. 1988). It is believed that this is a dynamically distinct regime in which the mesoscale variability is not dominated by radiating waves.

4. Observations

We seek to obtain observational evidence for baroclinic Rossby wave generation as a result of baroclinic instability of the CVFZ. Ideally, one would like to directly measure the three-dimensional velocity and vorticity fields as a function of time in order to firmly establish the character of the observed variability and relate it to a Rossby wave. Obviously the data required to do this would be extensive and no such dataset exists. We can, however, make use of our knowledge of Rossby wave dynamics and the characteristic behavior of the waves found in the numerical simulation to provide us with signatures by which the existence and source of the waves may be inferred. The sign of the Reynolds stress is a strong measure of the preferred orientation of the variability and an indication of the direction of energy propagation for waves in the system. Bower and Hogg (1991) used the sign of the Reynolds stress based on historical current-meter data to investigate the radiation of Rossby waves to the north and south of the Gulf Stream. Estimates of the observed Reynolds stress in the present analysis are obtained from both Lagrangian floats and moored current meters. The patterns of the real Lagrangian floats may also be compared with those calculated from the three-dimensional model fields, which we know to be representative of the Rossby wave variability in the model, for qualitative similarity. In addition, for variability dominated by wavelike motions, we expect to find a peak in the kinetic energy spectra representative of the frequency of such waves. Estimates of the energy spectra are available from both the Lagrangian floats and the moored current meters. Finally, we expect the eddy kinetic energy calculated from both the Lagrangian drifters and the current meters to be consistent with the expected amplitude of these Rossby waves.

a. Reynolds stress

A long-term Sound Fixing and Ranging (SOFAR) float experiment was carried out at the Mediterranean Water depth (1100 m) in the eastern basin of the North Atlantic between 1984 and 1988 (Zemanovic et al. 1988). SOFAR floats are designed to remain at a constant specified pressure, thus resisting changes in depth that would otherwise occur in regions of upwelling or downwelling. The simulated floats in the previous section undergo relatively small changes in depth over each cycle of the wave (relative to the vertical scale of the wave), so we believe that the horizontal trajectories of the SOFAR floats in such waves will represent well the actual horizontal trajectory that would be followed by a Lagrangian water parcel. Although most of the floats in this experiment were placed far to the north of the CVFZ, three floats are located far enough south to be relevant to the present study. The float trajectories are shown in Fig. 11, as in the model floats a small circle indicates the starting location of each float and + marks are placed at 60-day intervals along the float tracks. Float FA started at 24°N, 27°W and was tracked for a period of 4.4 years. Float FB was started in a meddy at 32°N, 22°W but after 2.8 years was ejected from the meddy near 22.5°N, 22°W. Only the remaining 1.6 years, which are shown in the figure, will be considered here. Float FC was started at 26°40′N, 26°W and was tracked for 4.4 years. The mean position, depth, Reynolds stress, and eddy kinetic energy for each of the floats is given in Table 1. The mean locations of each of the floats are indicated on the Reynolds stress map (Fig. 8) by triangles.

Each of the SOFAR floats found in this region exhibits a pattern similar to the simulated numerical model floats (cf. Fig. 10). There is a clear northwest-to-southeast orientation of the trajectories with meander amplitudes on the order of 200 km. Floats FA and FB undergo very little net translation over the total time series, while float FC appears to have both oscillations and a net translation to the northeast (similar to one such float from the model in this region). The Reynolds stress is negative for all three floats, varying between -0.33 cm^2 s^{-2} for float FB and -4.1 cm^2 s^{-2} for float FA. These values compare well with both the model-simulated float and the mean map of Reynolds stress calculated from the last three years of model integration.

Moored current meters also provide estimates of kinetic energy and Reynolds stresses. There are five cur-

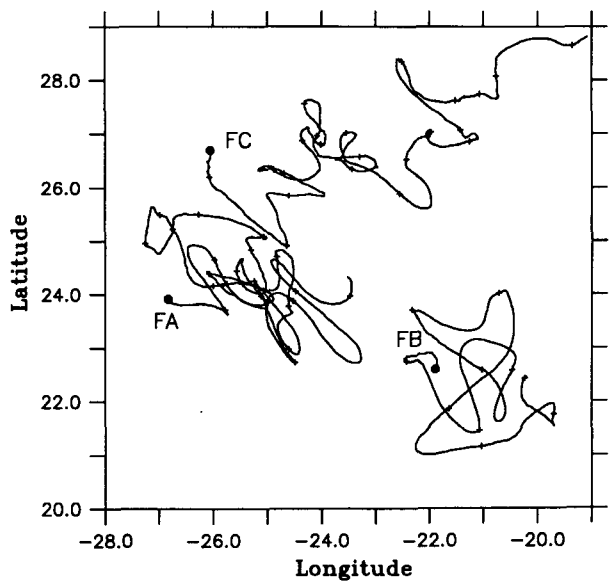

FIG. 11. Trajectories of three SOFAR floats, FA, FB, and FC.

rent meters in the vicinity of the CVFZ; their positions are indicated in Fig. 8 by the circles and statistics for each mooring are given in Table 1 (from the summary by Dickson 1989; the original data were collected at the Institut für Meereskunde an der Universität Kiel). The Reynolds stresses are negative for all four of the moorings placed to the north of the mean position of the CVFZ (M2–M5), while the single mooring to the south (M1) gives a positive value of the Reynolds stress. The amplitudes of the Reynolds stress terms are generally consistent with those calculated from the SOFAR and model float trajectories. The distribution of Reynolds stress is similar to that found in Fig. 8, with the two largest estimates found near the two local maxima in the mapped field and the positive value found to the south of the front.

Deep current meters near 4000 m at the same mooring locations give Reynolds stresses an order of magnitude lower with both positive and negative values to the north of the front. The lack of a coherent Reynolds stress signature at this depth may be explained if we consider the vertical propagation characteristics of the waves. It is believed that the source of the radiating waves is in the upper 2000 m because the velocity signature in the CVFZ is very weak below this depth in both observations (Zenk et al. 1991) and in the CME model. The vertical group velocity is approximately 1 km yr^{-1}, requiring two years for the signal to propagate from 2000 m to 4000 m. The horizontal group velocity is approximately 1 cm s^{-1} so that over these two years the wave would have traveled approximately 630 km in the horizontal, placing the waves well to the north of the mooring locations by the time the signal reached 4000-m depth.

b. *Eddy kinetic energy*

The eddy kinetic energies (K_E) of the SOFAR floats, listed in Table 1, vary between 3.9 cm^2 s^{-2} for float FC and 11.1 cm^2 s^{-2} for float FB. Peak float velocities of 4–6 cm s^{-1} occur as the floats are traveling along nearly straight paths oriented from northwest to southeast, the same as was found for the simulated floats. The amplitude of K_E at each mooring is also listed in Table 1. The values are between 6.1 cm^2 s^{-2} and 10.9 cm^2 s^{-2}. The K_E of the model float is 4.0 cm^2 s^{-2}, slightly less than, but close to, the observed values.

The kinetic energy spectra for the model-simulated float (F1) and each of the SOFAR floats (FA, FB, and FC) are shown in Fig. 12a. Floats F1 and FA show a clear peak in kinetic energy at 110 days. Floats FB and FC show two peaks, one at a slightly longer period of 135 days and one at a slightly lower period of 100 days. The model float kinetic energy decays somewhat more quickly at higher frequencies than do the SOFAR floats. This is expected, given the relatively modest horizontal resolution and strong eddy viscosity used in the model.

The kinetic energy spectra for mooring M2 are shown in Fig. 12b (redrafted from OK91). The energy spectra have a peak between 100 and 125 days. This frequency is in good agreement with the frequency of the simulated Rossby waves and also with the peak found in the kinetic energy spectra of the three SOFAR float trajectories, although the amplitude is somewhat lower. This may just be due to the fact that this mooring is a little deeper in the water column (1250–1410 m) and the baroclinic signal decreases with depth (by approximately a factor of 2 relative to 1000 m, see Fig. 4). The kinetic energy drops off very rapidly at higher frequencies and decreases slightly at lower frequencies.

The magnitude and spectra of K_E calculated from both the moored arrays and the SOFAR floats are consistent with what was calculated for the simulated float placed in the model Rossby wave. These results support the hypothesis that the observed variability is caused by radiating baroclinic Rossby waves, which were generated at the Cape Verde frontal zone.

It has been found that the K_E in the eastern basin of the CME model is generally much less than observed (S90; Treguier 1991) while the K_E of the individual Rossby wave identified here compares well with the observations. At the NEADS-1 mooring (33°N, 22°W) the K_E in the mesoscale frequency band (50 to 200 days) at 1000 m is found to be low by two orders of magnitude (Treguier 1991). The NEADS-1 mooring is located too far to the north to be influenced by the Rossby wave radiation mechanism identified in this study. The source of the mesoscale variability in that region is related to the local instability of the Azores Current and its recirculation (S90; Beckmann 1988). The mean K_E at 1125 m in the CVFZ is approximately 1 cm^2 s^{-2} to 2 cm^2 s^{-2} (S90), lower than the observations in Table 1 by a factor of 2–10. This lower value in the model could result from several things: the model may not be generating enough waves at the front, the waves that are generated may not be strong enough, the waves may decay prematurely, or the additional energy levels may be a result of some other mechanism not properly represented in the model. In the absence of more observations it is difficult to rule out any of these explanations. However, because the waves exist throughout the region in the model, it seems that the model is generating them quite regularly. The K_E of most of the waves is somewhat less than that for the wave which was chosen for detailed study here. These lower energy levels are probably a result of the horizontal grid spacing, which only marginally resolves the 300-km waves (approximately 9 grid points per wavelength) and the premature decay which would result from the viscous dissipation as the waves propagate away from the front. It is believed, however, that the model is capturing the essential process of wave radiation at the present resolution.

5. Conclusions

It is proposed here that the Cape Verde frontal zone (CVFZ) is a source of radiating Rossby waves. A con-

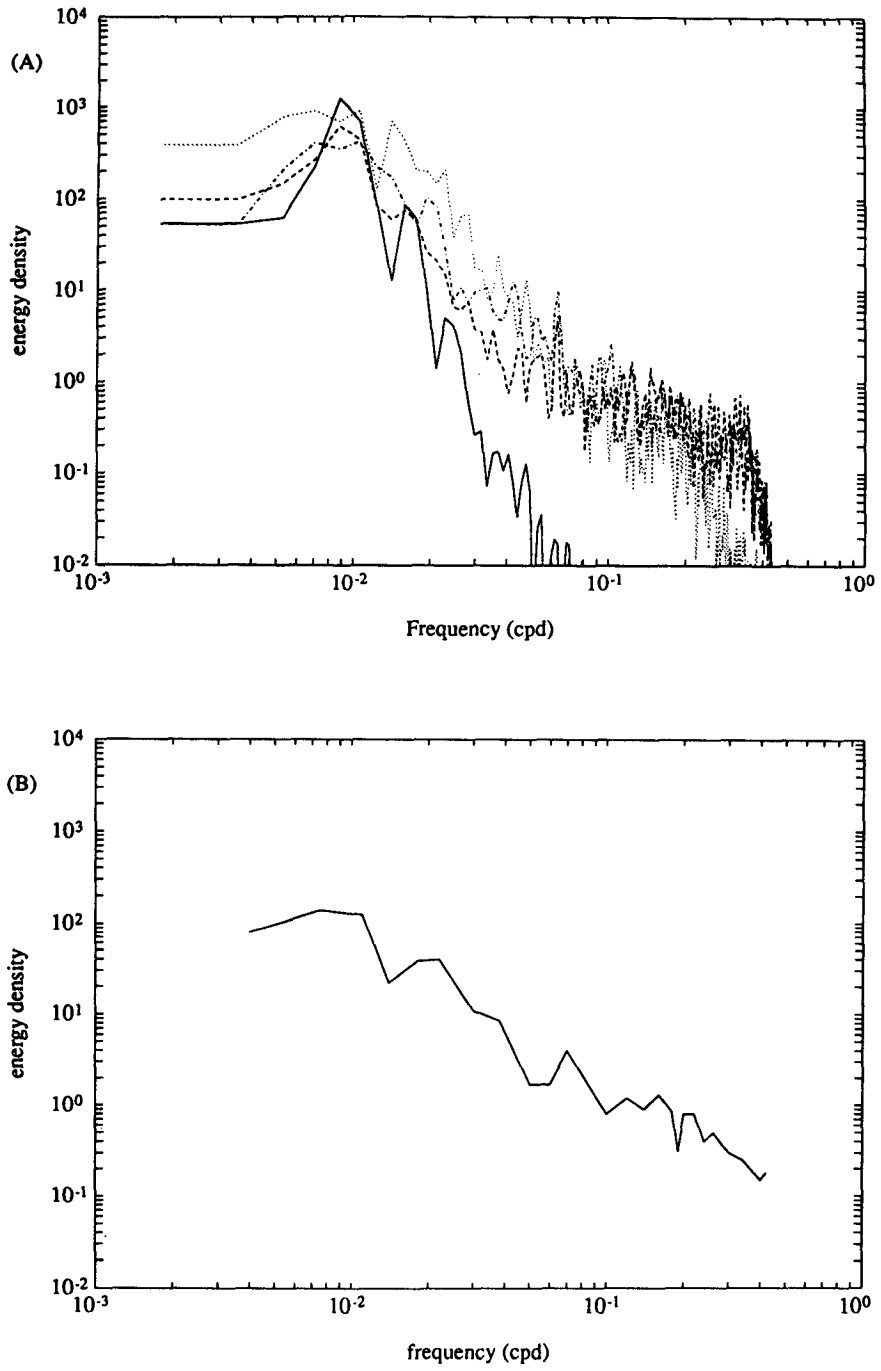

FIG. 12. Kinetic energy density ($cm^2\ s^{-2}\ cpd^{-1}$) for: (a) CME float F1 (solid line), SOFAR floats FA (dashed line), FB (dotted line) and FC (dot-dashed line), and (b) current meter M2 (redrafted from Onken and Klein 1991).

dition for waves to radiate away from a meandering front is that a wavelength and phase speed of the unstable modes match that of a freely propagating wave in the surrounding medium. A linear quasigeostrophic stability analysis indicates that an idealized CVFZ is unstable to westward-propagating waves at wavelengths between 100 km and 750 km. The phase speed of these unstable modes matches the first-mode baroclinic Rossby wave dispersion relation at a wavelength of 315 km and a phase speed of -3 cm s^{-1}, giving a period of 120 days.

Supporting evidence for the existence of these waves was obtained from the CME eddy-resolving general circulation model of the North Atlantic. Baroclinic

Rossby waves were identified at middepth in the southeastern basin through the leading-order balance in the vorticity equation terms. These waves were found to have wavelengths and frequencies that agreed well with that predicted by the linear theory. Simulated float trajectories were recovered from the Eulerian model data to reveal the Lagrangian signature of the wave packets. Floats within Rossby wave packets undergo large oscillations in a northwest–southeast (southwest–northeast) orientation for floats to the north (south) of the CVFZ, often with very little net translation. The large-scale distribution of float trajectories indicates that the Rossby waves are present throughout the region. The orientation of the float trajectories and the Reynolds stress calculated from the final three years of model data verifies that the source region of these waves is the CVFZ. The large number of waves present in the area suggests that they are being continuously generated at the front.

Although observations at middepths in this region are sparse, all of the available data known to us are consistent with our hypothesis that baroclinic Rossby waves are present in this region and that the source for these waves is the CVFZ. Several SOFAR float trajectories to the north of the front demonstrate Lagrangian signatures very similar to that calculated from the Rossby waves identified in the numerical model. In addition, the kinetic energy amplitude, spectra, frequency, and Reynolds stresses of the SOFAR floats are all in good agreement with that predicted by the linear theory and found in the numerically simulated floats. Five current meters, four to the north of the front and one to the south, give Reynolds stresses in good agreement with northward propagation to the north of the front and southward propagation to the south of the front. Kinetic energy spectra available for one of the current meters to the north of the front show a maximum close to the predicted Rossby wave frequency. The CME model was essential to the present analysis because it filled the gap between the very idealized linear stability analysis and the observations in such a way that we were able to relate the available information to the mechanism of Rossby wave radiation.

Because of the general agreement between the observed variability and the modeled Rossby waves, and the emergence of these waves as the major component of eddy kinetic energy in this region in the CME model, it is concluded that Rossby waves radiating from the CVFZ are a significant source of eddy kinetic energy at middepths in the southeastern basin of the North Atlantic.

Acknowledgments. Support for this work was provided by the National Science Foundation Grant No. OCE-9009463. The author would like to thank Drs. Jim Price and Phil Richardson for providing their SOFAR float data and helpful comments. The author is also grateful to Drs. William Holland and Frank Bryan for providing the Community Modeling Effort output. Dr. Nelson Hogg also provided helpful comments. Dr. Aike Beckmann is thanked for providing the solution procedure for the linear stability analysis. Many of the computations reported in this paper were carried out on the Cray YMP at the National Center for Atmospheric Research.

REFERENCES

Beckmann, A., 1988: Vertical structure of midlatitude mesoscale instabilities. *J. Phys. Oceanogr.*, **18,** 1354–1371.

Böning, C. W., and M. D. Cox, 1988: Particle dispersion and mixing of conservative properties in an eddy resolving model. *J. Phys. Oceanogr.*, **18,** 320–338.

Bower, A. S., and N. G. Hogg, 1992: Evidence for barotropic wave radiation from the Gulf Stream. *J. Phys. Oceanogr.*, **22,** 42–61.

Bryan, F. O., and W. R. Holland, 1989: A high resolution simulation of the wind- and thermohaline-driven circulation of the North Atlantic Ocean. *Proc. Hawaiian Winter Workshop: Parameterizations of small scale processes.* Honolulu, U.S. Office of Naval Research, Hawaii Institute of Geophysics, and the University of Hawaii.

Dickson, R., 1989: Flow statistics from long-term current-meter moorings the global data set in January 1989. [MAFF Directorate of Fisheries Research, Lowestoft, England] *World Meteorological Organization Technical Document No. 337,* 414 pp.

Hogg, N. G., 1988: Stochastic wave radiation by the Gulf Stream. *J. Phys. Oceanogr.*, **18,** 1687–1701.

Johns, W. E., and D. R. Watts, 1986: Time scales and structure of topographic Rossby waves and meanders in the deep Gulf Stream. *J. Mar. Res.*, **44,** 267–290.

Louis, J. P., B. D. Petrie, and P. C. Smith, 1982: Observations of topographic Rossby waves off the continental margin off Nova Scotia. *J. Phys. Oceanogr.*, **12,** 47–55.

Luyten, J. R., J. Pedlosky, and H. Stommel, 1983: The ventilated thermocline. *J. Phys. Oceanogr.*, **13,** 292–309.

Malanotte-Rizzoli, P., D. B. Haidvogel, and R. E. Young, 1987: Numerical simulations of transient boundary forced radiation. Part 1: The linear regime. *J. Phys. Oceanogr.*, **17,** 1439–1457.

Onken, R., and B. Klein, 1991: A model of baroclinic instability and waves between the ventilated gyre and the shadow zone of the North Atlantic Ocean. *J. Phys. Oceanogr.*, **21,** 53–67.

Pedlosky, J., 1977: On the radiation of meso-scale energy in the mid-ocean. *Deep-Sea Res.*, **24,** 591–600.

Shultz, J. R., 1987: Structure and propagation of topographic Rossby waves northeast of Cape Hatteras, North Carolina. M.S. thesis, University of North Carolina, 44 pp.

Spall, M. A., 1989: Regional primitive equation modeling and analysis of the POLYMODE data set. *Dyn. Atmos. Ocean.*, **14,** 125–174.

——, 1990: Circulation in the Canary Basin: A model/data analysis. *J. Geophys. Res.*, **95,** 9611–9628.

Tai, C-K., and W. B. White, 1990: Eddy variability in the Kuroshio Extension as revealed by satellite altimetry: Energy propagation away from the jet, Reynolds stress, and seasonal cycle. *J. Phys. Oceanogr.*, **20,** 1761–1777.

Talley, L. D., 1983: Radiating instabilities of thin baroclinic jets. *J. Phys. Oceanogr.*, **13,** 2161–2181.

Treguier, A. M., 1992: Kinetic energy analysis of an eddy-resolving primitive equation North Atlantic model. *J. Geophys. Res.*, **97,** 687–701.

Zemanovic, M. E., P. L. Richardson, J. R. Valdes, J. F. Price, and L. Armi, 1988: SOFAR float Mediterranean outflow experiment data from the second year, 1985–1986. Woods Hole Oceanographic Tech. Rep. WHOI-88-43:230, 239 pp.

Zenk, W., B. Klein, and M. Schröder, 1991: Cape Verde Frontal Zone. *Deep-Sea Res.*, **38**(Suppl.), 505–530.